Available online at www.jbr-pub.org.cn

Open Access at PubMed Central

The Journal of Biomedical Research, 2021 35(5): 395–407

JBR

Original Article

Pathogenesis and drug response of iPSC-derived cardiomyocytes from two Brugada syndrome patients with different $Na_v1.5$-subunit mutations

Yue Zhu[1,△], Linlin Wang[2,△], Chang Cui[1], Huiyuan Qin[1], Hongwu Chen[1], Shaojie Chen[1], Yongping Lin[1], Hongyi Cheng[1], Xiaohong Jiang[1], Minglong Chen[1,✉]

[1]*Department of Cardiology, the First Affiliated Hospital of Nanjing Medical University, Nanjing, Jiangsu 210029, China;*
[2]*Department of Cardiology, the Affiliated Brain Hospital of Nanjing Medical University, Nanjing Chest Hospital, Nanjing, Jiangsu 210029, China.*

Abstract

Brugada syndrome (BrS) is a complex genetic cardiac ion channel disease that causes a high predisposition to sudden cardiac death. Considering that its heterogeneity in clinical manifestations may result from genetic background, the application of patient-specific induced pluripotent stem cell-derived cardiomyocytes (iPSC-CMs) may help to reveal cell phenotype characteristics underlying different genetic variations. Here, to verify and compare the pathogenicity of mutations (*SCN5A* c.4213G>A and *SCN1B* c.590C>T) identified from two BrS patients, we generated two novel BrS iPS cell lines that carried missense mutations in *SCN5A* or *SCN1B,* compared their structures and electrophysiology, and evaluated the safety of quinidine in patient-specific iPSC-derived CMs. Compared to the control group, BrS-CMs showed a significant reduction in sodium current, prolonged action potential duration, and varying degrees of decreased V_{max}, but no structural difference. After applying different concentrations of quinidine, drug-induced cardiotoxicity was not observed within 3-fold unbound effective therapeutic plasma concentration (ETPC). The data presented proved that iPSC-CMs with variants in *SCN5A* c.4213G>A or *SCN1B* c.590C>T are able to recapitulate single-cell phenotype features of BrS and respond appropriately to quinidine without increasing incidence of arrhythmic events.

Keywords: human iPSCs, Brugada syndrome, disease modeling, quinidine, *SCN5A*, *SCN1B*

Introduction

Brugada syndrome (BrS) is an inheritable cardiac condition characterized by a typical electrocardiogram of right bundle branch block with ST-segment elevation in V1-V3[1]. BrS is associated with a high incidence of ventricular arrhythmia, which is prone to sudden cardiac death, especially in young men[2]. The implantation of a cardiac defibrillator (ICD) is the only established treatment[3]. However, shock from

△These authors contributed equally to this work.

✉Corresponding author: Minglong Chen, Department of Cardiology, the First Affiliated Hospital of Nanjing Medical University, 300 Guangzhou Road, Nanjing, Jiangsu 210029, China. Tel: +86-25-83781867. E-mail: chenminglong@njmu.edu.cn.

Received: 14 March 2021; Revised: 17 May 2021; Accepted: 25 May 2021; Published online: 22 July 2021

CLC number: R541.7, Document code: A

The authors reported no conflict of interests.

https://doi.org/10.7555/JBR.35.20210045

ICD is painful and may cause post-ICD shock stress reactions[4]. Alternatively, drugs that counteract the ionic current imbalance may be efficient. Currently, quinidine is applied in BrS patients to prevent the electrical storm of ICD, but its effectiveness and safety are controversial[5].

Genetic studies have revealed that BrS is associated with variations in multiple genes, including *SCN5A*, *SCN1B*, *CACNA1C*, and *KCND3*[6]. The most commonly involved gene in BrS is *SCN5A*, which encodes the α-subunit of the voltage-gated cardiac sodium channel ($Na_v1.5$)[7] and has been reported in more than 25% of BrS patients[8]. Recently, we reported that a single nucleotide variant (A197V) in *SCN1B*, encoding the β1-subunit of $Na_v1.5$, was responsible for BrS susceptibility[9]. Such loss of function of the sodium channel resulted in impaired depolarization and a prominent transient-outward current (I_{to})[10]. However, cardiac phenotype caused by *SCN1B* variation has been less reported using patient-specific induced pluripotent stem cell-derived cardiomyocytes (iPSC-CMs). Also, the characterization of cardiomyocytes with genetic variations in different subunits of $Na_v1.5$ remains to be compared.

Conventional heterologous expression provided insights into single-channel function, but fails to reflect the changes in whole membrane potential and electro-mechanical coupling. Thus, human cardiomyocytes, especially patient-specific cardiomyocytes, are needed to explore the mechanisms underlying the ion channel diseases. Indeed, human iPSCs provide a promising tool for recapitulating the phenotype of cardiac disease and for evaluating the efficiency of drug treatments[11–13]. In recent years, case studies demonstrated that BrS patient-specific iPSC-CMs are accurate disease models *in vitro*[14–15]. However, their drug responses to quinidine have not been fully elucidated.

In the present study, we recruited two Brugada patients who carried *SCN5A* c.4213G>A and *SCN1B* c.590C>T, respectively. We generated patient-specific iPS cell lines and differentiated them into ventricular cardiomyocytes. Through structural and electrophysiological assessments, we investigated the pathological properties of BrS at the cellular level. By evaluating the drug responses to quinidine *in vitro*, we highlighted the efficacy and safety of quinidine treatment in BrS-CMs.

Materials and methods

Generation of human iPS cell lines

Human iPS cell lines used in this study were derived from peripheral blood mononuclear cells of two Brugada patients and one healthy volunteer. The approval of the study was provided by the Bioethics Committee of the First Affiliated Hospital of Nanjing Medical University (2014-SR-090). The iPSC lines were generated using a CytoTune-iPS 2.0 Sendai reprogramming kit (Thermo Fisher Scientific, USA), which employed four Yamanaka factors (OCT4, KLF4, SOX2, and cMYC), following the manufacturer's instructions with subtle adjustments. Reprogrammed PBMCs were replated onto Matrigel (Corning, USA) coating plates, and the medium was changed to mTeSR1 (STEMCELL Technologies Inc., Canada) after transduction. Individual colonies were identified on day 7, picked 20 days later, and maintained in mTeSR1 medium. Another control iPS cell line was purchased from Wicell (iPS-DF6-9-9T, WiCell Research Institute, USA).

Genome sequencing

To confirm the presence of the variations in the two iPS cell lines, patient-derived iPSCs were examined by Sanger sequencing. Total DNA was isolated using a TIANamp genomic DNA kit (Tiangen Biotech, China), and the coding regions of *SCN5*A and *SCN1B*, including each variation site, were amplified by PCR. The PCR products were purified using a DNA purification kit (Tiangen Biotech) and then were sequenced. The results were compared with the *SCN5A* and *SCN1B* reference sequences NM_001099404 and NM_001037.

Differentiation of iPSC-CMs

Briefly, iPSCs were allowed to grow to over 90% confluence in mTeSR1 medium and then were switched to RPMI 1640 medium (Thermo Fisher Scientific) containing B-27 supplement without insulin (Thermo Fisher Scientific). On day 0 to 1, additional CHIR-99021 (6 μmol/L, Selleckchem, USA) was added to induce mesodermal differentiation. On day 3 to 4, IWR-1 (5 μmol/L, Sigma-Aldrich, Germany) was added to the medium to inhibit Wnt signaling and induce cardiogenesis. From day 5 to 7, BMS493 (1 μmol/L, Sigma-Aldrich) was added for directly differentiating into ventricular cardiomyocytes. From day 8 onwards, cells were cultured in RPMI 1640 containing B27 complete supplement (Gibco), and the medium was refreshed every other day. Beating cardiomyocytes were observed on day 8 to 10. Besides, to obtain enriched cardiomyocyte populations, glucose-free DMEM supplemented with 4 mmol/L lactate medium (Sigma-Aldrich) and 3.6 mmol/L HEPES (Sigma-Aldrich) were applied for 4 days. Cells for further functional

and electrophysiological analyses were cultured for at least 60 days and dissociated using 0.25% trypsin-EDTA.

Flow cytometry analysis

Cells were treated with the appropriate dissociation solution (Accutase for iPS cells, 0.25% trypsin for CMs), fixed with 4% paraformaldehyde, and permeated with 0.1% Triton X-100 at room temperature. Pluripotent stem cells were counted and stained using phycoerythrin conjugated antibodies against SSEA-4 (1:50 dilution; Miltenyi Biotec, Germany) for 30 minutes at 4 °C shielded from light. Cardiomyocytes were co-incubated with anti-cTnT-FITC (1:50 dilution; Miltenyi Biotec) and anti-MLC2v-PE (1:50 dilution; Miltenyi Biotec) in PBS at 4 °C for 30 minutes. REA Control-FITC (1:50 dilution; Miltenyi Biotec) and REA Control-PE (1:50 dilution; Miltenyi Biotec) were used as isotype controls. The cells were measured using FACSCalibur (BD, USA) and subsequent analyses were performed using FlowJo software (Tree Star, version 10.5.3).

Immunofluorescence staining

Cells were seeded on a coverslip and cultured for 3 to 5 days before being fixed in 4% paraformaldehyde for 20 minutes. The cells were permeabilized with 0.1% Triton X-100 for 5 minutes when needed. Cells were then blocked in 5% BSA in PBS for 30 minutes; all these procedures were performed at room temperature. Cells were then incubated overnight at 4 °C with primary antibodies. For pluripotent stem cells, anti-SSEA4 (1:200 dilution; Abcam, UK) and anti-Nanog (1:200 dilution; Abcam) were applied. For cardiomyocytes, anti-α-actinin (1:200 dilution; Sigma-Aldrich), anti-cardiac troponin I (1:200 dilution; Abcam), and anti-Nav1.5 (1:100 dilution; Abcam) were used. The following secondary antibodies included Alexa Fluor 488 goat anti-rabbit IgG (1:800 dilution; Abcam) and Alexa Fluor 555 goat anti-mouse IgG (1:800 dilution; Abcam) were incubated with samples at room temperature for 30 minutes. The nuclei were stained with DAPI (Life Technologies, USA). Then, the cells were rinsed with PBS and observed under a fluorescence microscope (Axio Imager A2, Carl Zeiss, Germany). Images were analyzed and merged with ImageJ (NIH, version 1.8.0_77).

Transmission electron microscopy

CMs were dissociated into single cells with 0.25% trypsin. Samples were then fixed with 2.5% glutaraldehyde (Sigma-Aldrich), postfixed with 1% osmium tetroxide, and rinsed with PBS. After dehydration with a series of ethanol solutions and embedding into resin, ultrathin sections were cut with an ultramicrotome (EM UC7; Leica, Germany) and stained with lead citrate. Visualization was performed under a transmission electron microscope (JEM-1010, Jeol Ltd., Japan) equipped with a CCD camera operated at 75 kV.

Real-time reverse transcriptase PCR

Total RNA was prepared from CMs using TRIzol (Invitrogen) following the manufacturer's protocol. RNA (500 to 1000 ng) was reverse-transcribed into cDNA using iScript cDNA Synthesis Kit (Bio-Rad, USA). cDNA was then determined by the applied biosystems 7900HT fast real-time PCR system (ABI) with Hieff qPCR SYBR green master mix (Yesen-bio, China). The mRNA expression levels were normalized to the housekeeping gene *GAPDH* and *LMNA*. Primers used are summarized in ***Supplementary Table 1*** (available online).

Patch-clamp analysis

Cells at day 60 in independent differentiation batches and different culture dishes were used to evaluate electrophysiological properties. Three to 4 days after dissociation, single-cell patch-clamp experiments were performed using an Axopatch 200B amplifier (Axon Instruments, USA) and analyzed with Clampfit 10.3 software (Molecular Devices). Glass pipettes were pulled using borosilicate glass (Sutter Instrument, USA) and a micropipette puller (Model P-100, Sutter Instruments). Pipettes with resistance ranging from 2 to 4 MΩ were perfused with specified intracellular solutions and were used.

Na measurement

The sodium currents (I_{Na}) of cardiomyocytes were recorded using a whole-cell patch-clamp technique at room temperature. Data were filtered at 2 kHz and acquired at 20 kHz. I_{Na} was examined using the following intracellular solution designed to eliminate the outward potassium current: 10 mmol/L NaCl, 60 mmol/L CsCl, 60 mmol/L CsF, 10 mmol/L TEA-Cl, 1 mmol/L $CaCl_2$, 1 mmol/L $MgCl_2$, 10 mmol/L EGTA, 10 mmol/L glucose, and 10 mmol/L HEPES (pH 7.2 with CsOH). The external bath solution composition was as follows: 130 mmol/L choline chloride, 10 mmol/L NaCl, 1 mmol/L TEA-Cl, 1.8 mmol/L $MgCl_2$, 1.8 mmol/L $CaCl_2$, 0.2 mmol/L NiCl, 10 mmol/L glucose, and 10 mmol/L HEPES (pH 7.2 with NaOH). Nifedipine was added to exclude inward calcium current. The protocol for recording I_{Na} ranged

from –80 to +40 mV in 10 mV increments that occurred every 50 milliseconds. Cell capacitance was measured to normalize I_{Na} by applying a 10 mV voltage step from –100 mV, and current density was calculated as peak current divided by cell capacitance (pA/pF).

Voltage clamp recordings of I_{to} currents

I_{to} regulates phase 1 repolarization to modulate the early AP plateau. Here, I_{to} currents were recorded in extracellular solution that contained the following: 140 mmol/L NaCl, 5.4 mmol/L KCl, 1.8 mmol/L $CaCl_2$, 1 mmol/L $MgCl_2$, 0.33 mmol/L NaH_2PO_4, 10 mmol/L HEPES, and 10 mmol/L glucose (pH 7.4 with NaOH). The pipettes were filled with an internal solution that contained the following: 90 mmol/L K-aspartate, 45 mmol/L KCl, 5 mmol/L Na-pyruvate, 5 mmol/L MgATP, 5 mmol/L EGTA, 10 mmol/L HEPES, and 10 mmol/L glucose (pH 7.2 with KOH). I_{to} was determined by increasing the testing potential stepwise from –40 to 40 mV in 10 mV steps from a holding potential of –90 mV with a 20-millisecond pre-pulse to –35 mV to inactivate I_{Na}.

Action potential measurement

Action potentials were recorded at 37 °C in Tyrode's solution. Data were filtered at 5 kHz and digitized at 40 kHz. Pipettes were filled with the following internal solution (in mmol/L): 150 KCl, 5 NaCl, 2 $CaCl_2$, 5 Mg ATP, 5 HEPES, 5 EGTA, and 10 glucose (pH 7.2 with KOH). Extracellular solution contained: 135 mmol/L NaCl, 5.4 mmol/L KCl, 1.8 mmol/L $CaCl_2$, 1 mmol/L $MgCl_2$, 0.33 mmol/L NaH_2PO_4, 10 mmol/L HEPES, and 10 mmol/L glucose, adjusted to pH 7.4 with NaOH. APs were characterized by resting membrane potential (RMP), maximum AP amplitude (APA), maximum upstroke velocity (V_{max}), and average action potential duration (APD) at 90%, 50%, and 30% repolarization (APD90, APD50, and APD30, respectively). Each average data was from 10 consecutive recorded APs.

Calcium transient

Cells were loaded with the calcium-sensitive dye fluo-4 AM (Life Technologies) at a working concentration of 5 μmol/L for 60 minutes at 37 °C. Having been rinsed the iPSC-CMs, they were maintained in Tyrode's solution. The spontaneous calcium fluorescence signal was recorded by an inverted fluorescence microscope (Axio Vert A1, Carl Zeiss, Germany) equipped with an sCMOS camera (Tucsen, Dhyana95, China). The excitation and emission wavelengths of Fluo-4 were 488 nm and 505 nm, respectively. Recordings were obtained at the acquisition rate of 25 frames/second for a 15-second duration. To calibrate the cell-to-cell variability and background disturbance, the fluorescence intensity in the region of interest was determined based on the formula: (F-F0)/F0. Herein, F0 represents the baseline intensity, while F represents the intensity at any point in time. The parameters that describe and evaluate the calcium transient include the spontaneous beat rate, amplitude, and arrhythmic events that are EAD-like or fibrillation-like. Data were analyzed using ImageJ.

Drug response

Quinidine (Selleckchem) was dissolved in dimethyl sulfoxide to prepare a 100 mmol/L stock solution. Working solutions were freshly prepared in cell-specific medium. Final concentration was set as 0.1-fold to 10-fold the ETPC (unbound effective therapeutic plasma concentration) of quinidine (0.3, 1, 3, 10, and 30 μmol/L). Dilution ratio up to 1000 had no effect on cell apoptosis or cardiac electrical activity.

Baseline AP was recorded for each cell before the treatment. Then, quinidine was sequentially applied from the lowest to highest concentration at 10-minute intervals for washout to obtain a steady state. For each concentration, 10 recorded APs from each cell were averaged for analysis. The following parameters were quantitated as mentioned above: RMP, APA, V_{max}, APD30, APD50, and APD90. Recordings at each concentration were normalized to their baseline.

Statistical analysis

Data with a normal distribution were presented as the mean±SEM. Student's *t*-tests were then used in comparisons where there were two groups. The Chi-square test was used for categorical variables. For pharmaceutical experiments, the post-drug effects were evaluated by comparing to the baseline using a paired Student's *t*-test. All statistical analyses were performed with SigmaPlot 12.5 and GraphPad Prism 8 (GraphPad Software, USA) and significance was determined at a $P<0.05$.

Results

Clinical and genetic profiles

Two BrS patients and one healthy volunteer were recruited. The diagnosis of Brugada syndrome was made based on the 2005 consensus diagnostic criteria[16]. Patient 1 (BrS-SCN5A) was a 42-year-old man presenting with unstable ventricular tachycardia after multiple episodes of recurrent syncope. His resting ECG showed a characteristic type 1 Brugada pattern (***Fig. 1A***). Moreover, pedigree investigation showed that his brother died from sudden cardiac

death. Patient 2 (BrS-SCN1B) was a 46-year-old man with a history of recurrent syncope. The resting ECG exhibited typical type 1 Brugada ECG pattern (***Fig. 1B***). Both patients received ICD implantation and close follow-up. Genetic testing revealed a *SCN5A* c.4213G>A (V1405M) variation in BrS-SCN5A and a *SCN1B* c.590C>T (A197V) variation in BrS-SCN1B. The corresponding positions of each variation on the protein structure of the $Na_v1.5$ sodium channel α subunit or β-1 subunit are illuminated in ***Fig. 1C***.

Our healthy control subject (Control 1) was a 44-year-old young woman with normal ECGs and without personal or family history of sudden death. Whole-genome sequencing indicated no disease-causing variants in any cardiovascular-related genes. Another control cell line (Control 2) was generated from a healthy male.

Characterization of iPS cell lines

Human iPSCs were generated from PBMCs derived from the two patients and the healthy control. To verify the pluripotency of each iPS cell line, undifferentiated stem cells were fixed and stained. As expected, the cells in both the BrS and control groups expressed the robust pluripotency markers NANOG and SSEA4 (***Fig. 2A*** and ***Supplementary Fig. 1A***, available online). Further flow cytometry analysis revealed a high proportion (>95%) of SSEA-4-positive cells in each group (***Fig. 2B*** and ***Supplementary Fig. 1B***, available online). Genetic testing confirmed the variation sites of *SCN5A* c.4213G>A and *SCN1B* c.590C>T in the corresponding iPSC lines, indicating that reprogramming maintained the genetic variations found in the BrS patients (***Fig. 2C***). Also, relevant variations in control lines were not observed *via* Sanger sequencing (***Supplementary Fig. 1C***).

Structural analysis of BrS-CMs

Highly efficient cardiac differentiation was conducted. FACS analysis of the cardiac-specific marker cTnT and ventricular cardiomyocyte marker MLC2 confirmed the purity of ventricular myocytes to be over 90% (***Fig. 2D***). Considering the immaturity of

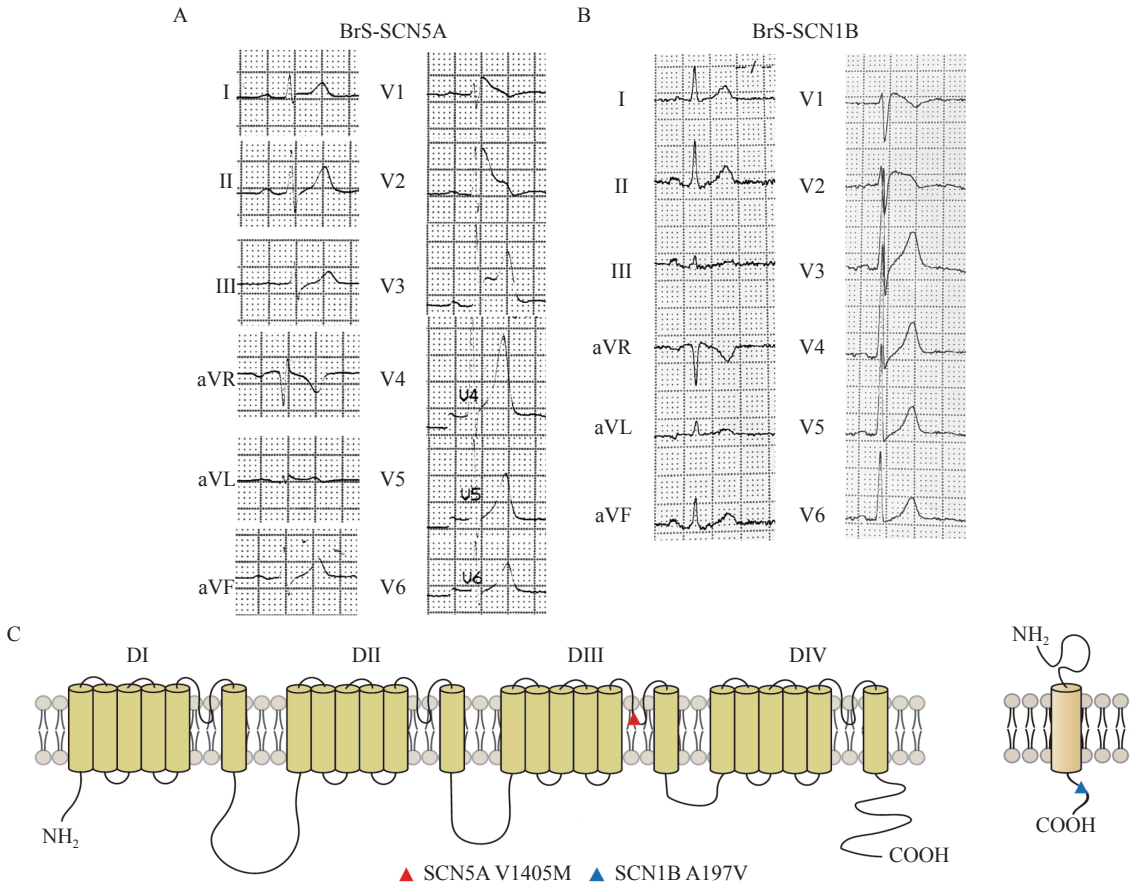

Fig. 1 **Clinical and genetical profile of the two Brugada syndrome patients.** A and B: Electrocardiograms of both patients show the typical ST segment elevation, a typical pattern of BrS. C: The corresponding positions of V1405M mutation on the protein structure of voltage-gated sodium-channel α subunit gene (left panel), and A197V mutation on the ß1 subunit gene (right panel). BrS: Brugada syndrome.

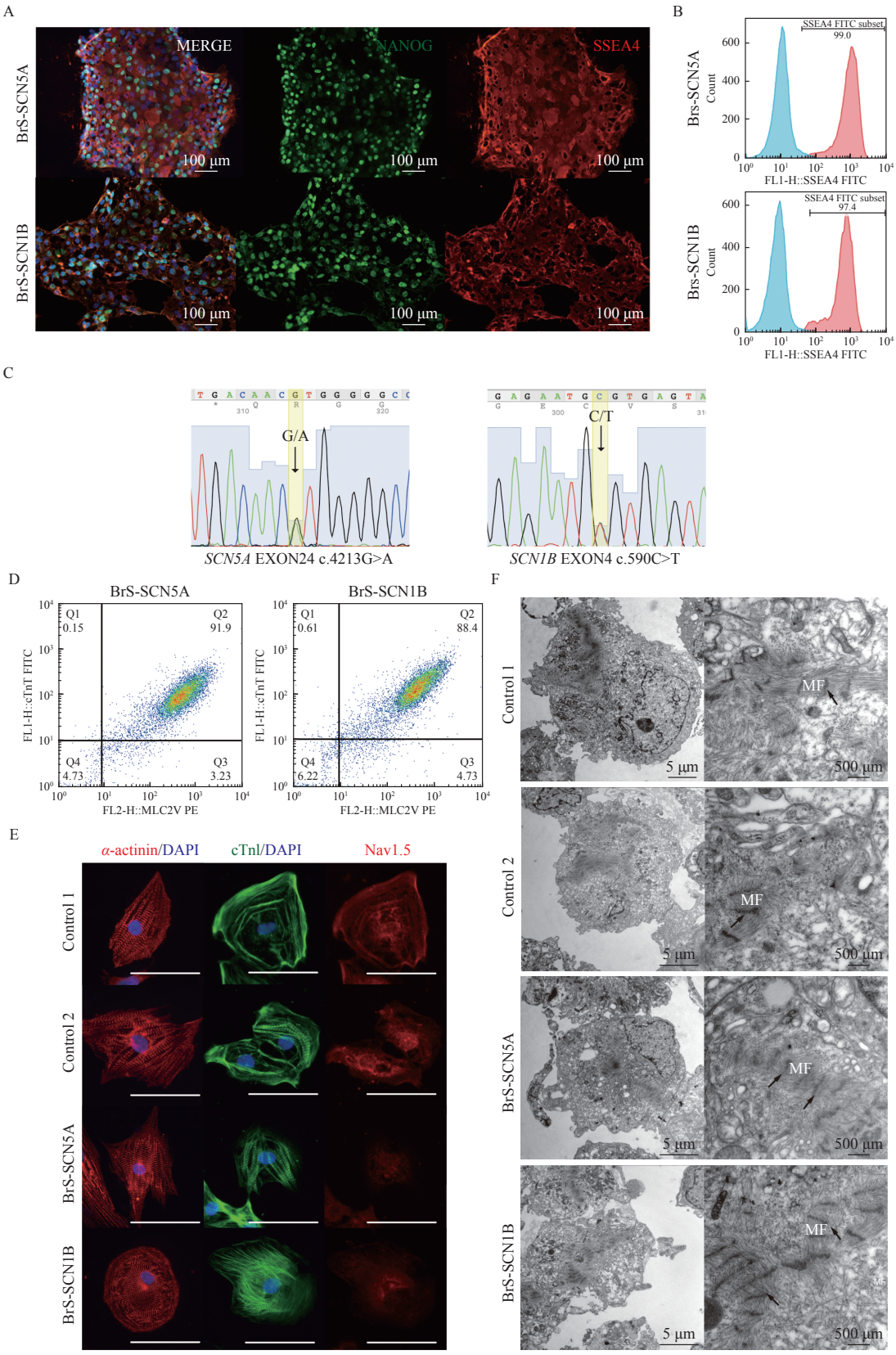

Fig. 2 **Characterization of iPSC lines and differentiated cardiomyocytes.** A: Images of iPS cells stained with pluripotency markers NANOG (green), SSEA4 (red) for BrS-SCN5A and BrS-SCN1B iPS cell lines. Nuclei were stained with DAPI (blue). Scale bars, 100 μm. B: Flow cytometry analysis of pluripotency markers (SSEA4) in generated BrS iPSC lines. C: Genotyping of BrS-SCN5A and BrS-SCN1B iPSC lines focusing on the loci around each mutation confirmed by DNA sequencing. D: Representative flow cytometry confirming the high percentage of ventricular myocytes in differentiated cells. E: Immunostaining of sarcomeric α-actinin, cTnI, and $Na_v1.5$ at 60 days post differentiation. Scale bars, 50 μm. F: TEM images of myofibrillar organization in control and BrS iPSC-CMs. Black arrow indicates z-lines. iPSC: induced pluripotent stem cell; TEM: transmission electron microscopy.

newly differentiated cardiomyocytes, prolonged cultivation up to 60 days was applied. To compare the morphological properties of the cells, we stained age-matched cells for cardiac structural proteins α-actinin and cTnI. All cells exhibited robust expression of these markers with organized striation patterns of sarcomeres (***Fig. 2E***). Besides, the staining of $Na_v1.5$ indicated the expression of $Na_v1.5$ was markedly reduced in BrS cells (***Fig. 2E***). Furthermore, we examined the cardiac ultrastructure using transmission electron microscopy. In both BrS and control iPSC-CMs, myofibrils were well organized with aligned linear Z-discs (***Fig. 2F***). Abundant mitochondria and sarcoplasmic reticulum could be seen around the sarcomere. Given the above findings, we reported no significant discrepancy in morphology between control and both BrS cardiomyocytes.

BrS-CMs showed impaired Na^+ current

To compare the impact of different variations in the $Na_v1.5$ subunits on sodium current, we measured the sodium current using voltage clamp experiments. ***Fig. 3A*** plots representative I_{Na} traces for BrS and control cardiomyocytes at varying potentials. It demonstrated a loss of function of the sodium channel current in both the BrS-SCN1B and BrS-SCN5A groups compared to control-derived cardiomyocytes (***Fig. 3B***). Further analysis demonstrated that peak I_{Na} density was reduced by 80% in BrS-SCN5A and 70% in BrS-SCN1B compared to their control counterparts (P<0.001 for both, ***Fig. 3C***), which was in line with the downregulation in relevant gene expression (P<0.001 for both, ***Fig. 3D*** and ***E***). Notably, the peak I_{Na} density of BrS-SCN5A cardiomyocytes was even

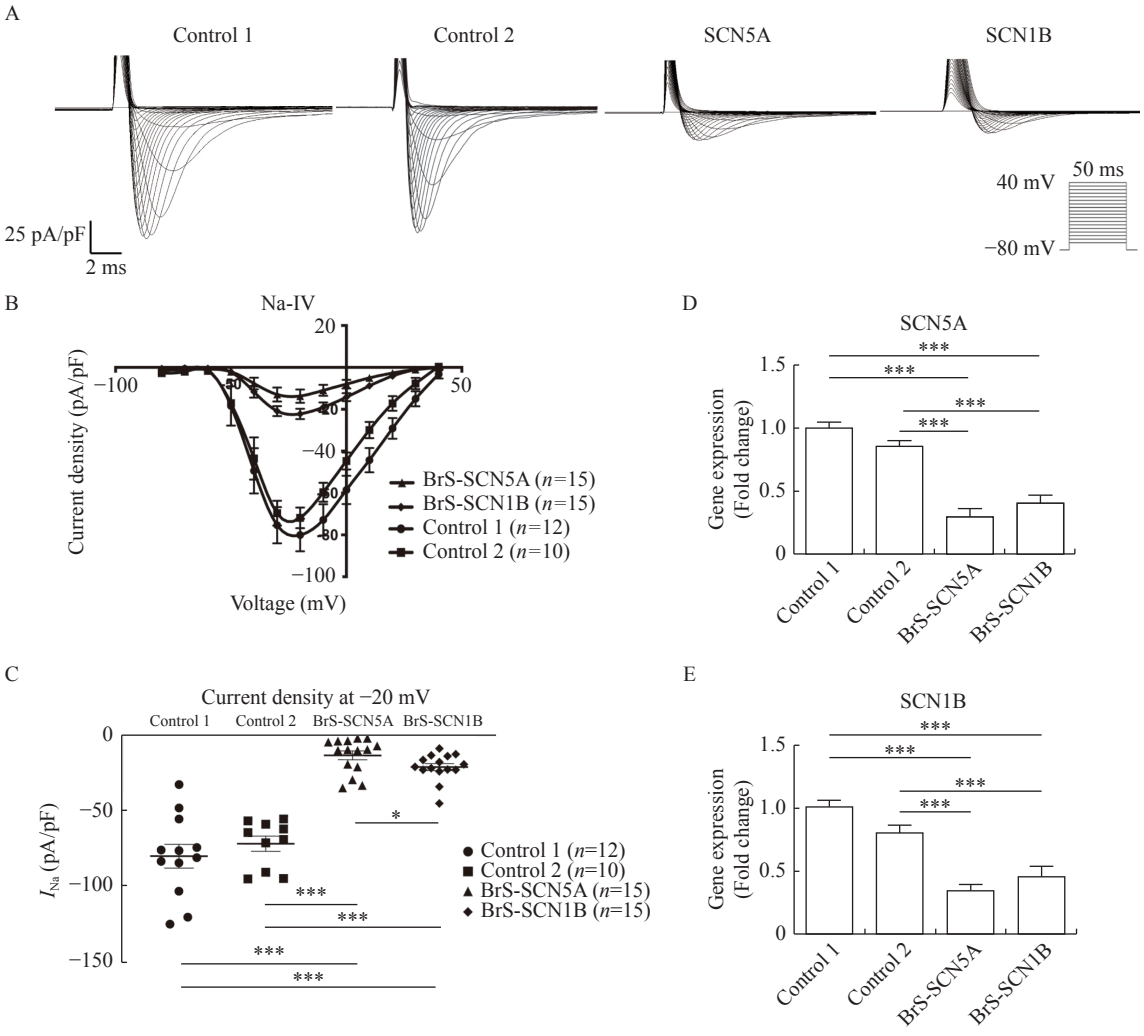

Fig. 3 **iPSC-CMs carrying *SCN5A* or *SCN1B* mutation showed impaired I_{Na} properties.** A: Typical I_{Na} curve measured by the voltage clamp protocol. Traces for pulses from −80 to −40 mV are shown. B: Current-voltage relationships of I_{Na} from Control 1 (n=12), Control 2 (n=10), BrS-SCN5A (n=15), and BrS-SCN1B (n=15) normalized to the cell capacitance. C: Comparison of I_{Na} density at −20 mV between control lines and the BrS lines. D and E: *SCN5A* and *SCN1B* expression evaluated by real-time RT-PCR (n=6 for each line). Data are presented as mean±SEM. Comparisons between two groups were analyzed using Student's t-test. $^{***}P$<0.001, $^{*}P$<0.05. iPSC-CMs: induced pluripotent stem cell-derived cardiomyocytes; I_{Na}: sodium current.

lower than that of the BrS-SCN1B group (P=0.02). In addition, we assessed the transient outward current (I_{to}), which was judged as another potential contributing factor of BrS. The results demonstrated that I_{to} currents were not significantly changed in either BrS cell line compared with the control (***Supplementary Fig. 2***, available online).

BrS-CMs exhibited abnormal action potential

To investigate whether $Na_v1.5$ variations would affect the whole membrane potential, we next recorded action potentials by patch-clamp. Only ventricular cardiomyocytes were studied in the present study (***Fig. 4A***)[13]. In line with our sodium current data, APA (***Fig. 4B***) and V_{max} (***Fig. 4C***) were

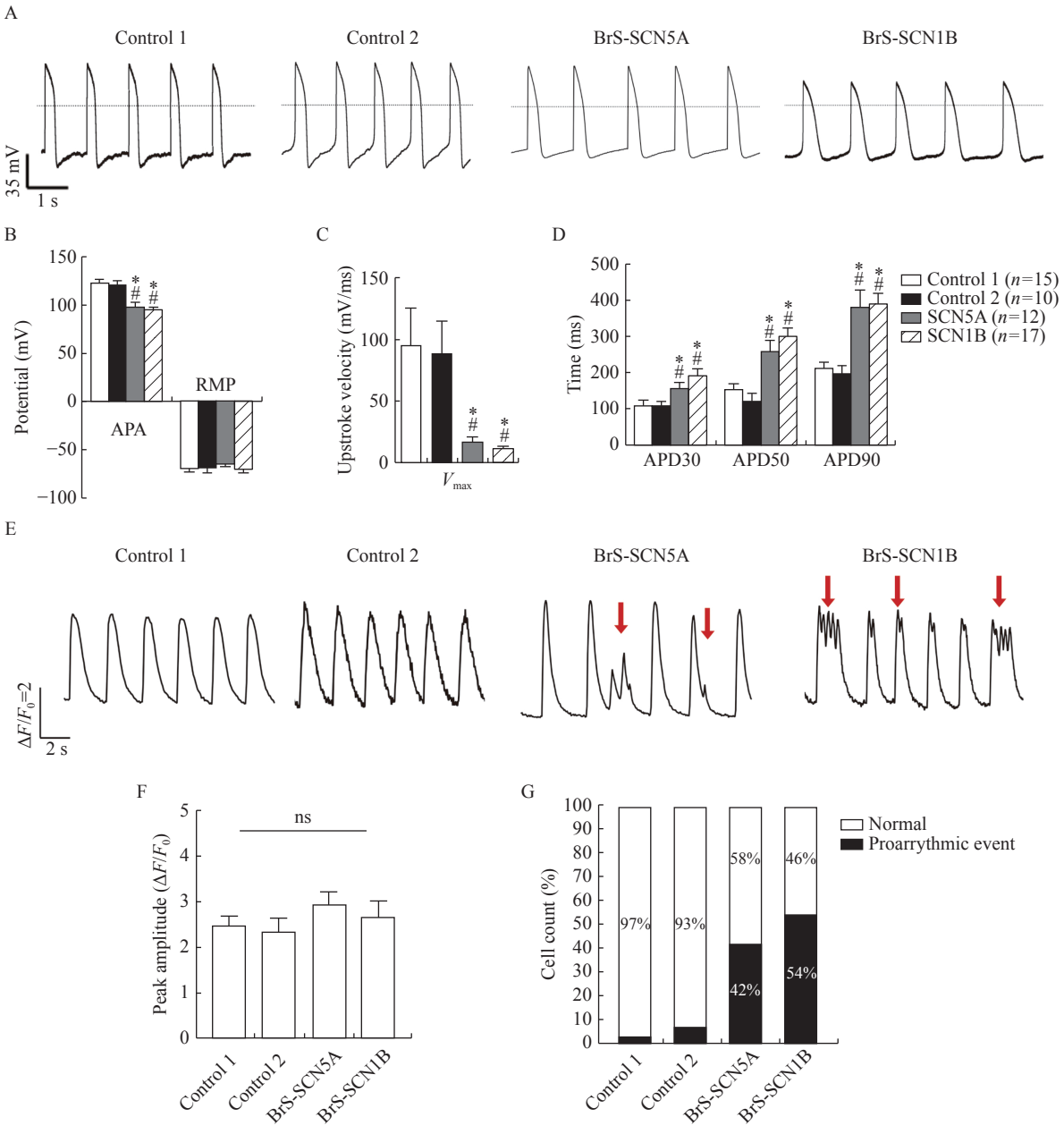

Fig. 4 **Both BrS iPSC-CMs exhibited prolonged action potential durations, decreased V_{max} and abnormal Ca^{2+} handling.** A: Representative spontaneous AP traces in control and BrS myocytes using current-clamp recording. Dotted line indicates 0 mV. B–D: Mean values for APA, RMP, V_{max}, and APD at 30%, 50%, and 90% repolarization (APD30, APD50, and APD90). Control1: n=15; Control2: n=10; BrS-SCN5A: n=12; BrS-SCN1B: n=17. $^{*}P$<0.01 *vs.* Control 1; $^{\#}P$<0.01 *vs.* Control 2. Data are presented as mean±SEM. Comparisons between two groups were analyzed using two-sided Student's t-test. E: Representative spontaneous Ca^{2+} transients, red arrow indicates irregular Ca^{2+} waveforms. F: Peak amplitude of spontaneous Ca^{2+} transients in control and BrS iPSC-CMs (n=30 for each line, Student's t-test). Ns: No significance (P>0.05). G: Proportions of cells showing proarrhythmic events in each line (n=30 for each line, Chi-square test). iPSC-CMs: induced pluripotent stem cell-derived cardiomyocytes; APA: action potential amplitude; RMP: resting membrane potential; V_{max}: maximum upstroke velocity; APD: action potential duration.

significantly decreased in the BrS groups compared to the control group (APA: $P<0.001$ for each comparison, V_{max}: $P<0.05$ for each comparison). Action potential durations (APD 30, 50, and 90) were significantly longer in both BrS cell groups than they were in the healthy control ($P<0.001$ for all groups, ***Fig. 4D***). To sum up, these results indicated that BrS iPSC-CMs exhibited notably aberrant AP phenotypes. Meanwhile, the action potentials from the BrS-SCN1B and BrS-SCN5A groups presented the same pattern. All the AP characterizations are summarized in ***Supplementary Table 2*** (available online).

BrS-CMs exhibited altered Ca^{2+} handling

Considering that calcium is a critical mediator of excitation-contraction coupling in cardiac cells, we then examined the changes in intracellular calcium concentration using calcium probes. The representative curves of Ca^{2+} handling from each group are shown in ***Fig. 4E***. Both BrS iPSC-CMs exhibited similar peak amplitudes, compared to control cells (***Fig. 4F***). Nevertheless, the kinetic stability of calcium handling was disturbed in the BrS groups. As shown in ***Fig. 4E***, BrS cells exhibited more proarrhythmic events, including delayed afterdepolarization-like and early afterdepolarization-like events, than controlled CMs. The percentages of cells showing proarrhythmic events in BrS-SCN5A, BrS-SCN1B, Control 1 and Control 2 lines were 58%, 46%, 3%, and 7%, respectively, $P<0.001$ for Chi-square test (***Fig. 4G***).

Cardiac safety evaluation of quinidine using BrS-CMs

Quinidine is a class 1A antiarrhythmic drug with significant I_{to} blocking properties. It was once expected to be efficient based on positive results in limited series of BrS patients[17] but other studies failed to demonstrate its beneficial effects[18–19]. In our cases, oral quinidine therapy was applied to both BrS-SCN5A and BrS-SCN1B patients after their ICD implantation. During follow-up, there was no report of ICD discharge in these two patients. Meanwhile, quinidine also blocked potassium channels in phase 3. Recent studies reported that quinidine-induced QT prolongation increased the risk of fatal arrhythmia[20]. Hence, further investigation of drug safety is warranted before the prescription of lifetime drug use.

Human iPSC-CMs are considered as precise tools for cardiac safety drug screening *in vitro*[21]. To further confirm the drug safety of quinidine in cells with these two variations, iPSC cardiomyocytes were subjected to quinidine at concentrations ranging from 0.3 to 30 μmol/L. The results demonstrated that quinidine had no impact on cell viability when examined by CardioExcyte 96 (Nanion Technologies, USA; ***Supplementary Fig. 3***, available online). Action potential was further analyzed to detect drug effects on cellular electrophysiology. As shown in ***Fig. 5A–G*** and ***Supplementary Table 3*** (available online), quinidine decreased the V_{max}, APA, and RMP in a concentration-dependent manner among the three groups. Interestingly, APD90 was prolonged in all cell lines as quinidine concentration increased, and then showed a downward trend when the concentration reached 3-fold the ETPC (10 μmol/L) or higher. Besides, the control group had a greater prolongation of APD90 than both BrS groups ($P=0.014$ for BrS-SCN5A, $P<0.001$ for BrS-SCN1B). All the groups showed similar mild changes in both APD30 and APD50. In addition, compared to the control group, both BrS groups displayed a higher incidence of arrhythmic events at baseline, including early afterdepolarizations (EADs) or delayed afterdepolarizations (DADs) (0 out of 10 for control, 3 out of 10 for BrS-SCN5A, 2 out of 9 for BrS-SCN1B). After treated with quinidine within 3-fold the ETPC, both BrS-CMs eliminated spontaneously occurring triggered events (***Fig. 5H*** and ***I***). These results highlighted that quinidine had positive effects in BrS-CMs with insurance of safety.

Discussion

BrS is an inheritable ion channelopathy associated with a propensity to fetal ventricular arrhythmias. Herein, we identified two novel mutations (*SCN5A* c.4213G>A and *SCN1B* c.590C>T) from two BrS patients, verified and compared their pathogenic phenotypes. Our results demonstrated that iPSC-CMs derived from different genotypes of BrS patients showed similar patterns, including the prolongation of APD, impairment of I_{Na}, and high prevalence of proarrhythmic events. Although many patient-specific iPS-CM models have been generated to recapitulate Brugada syndrome at the cellular level (***Supplementary Table 4***, available online), none has assessed the cellular response to quinidine, a controversial drug for BrS treatment. Here, our study provided a comprehensive evaluation of quinidine on BrS-CMs, supporting the safety of the drug for lifelong use.

Relatively mature phenotype by prolonged cultivation of iPSC-CMs

It is well known that newly differentiated iPSC-

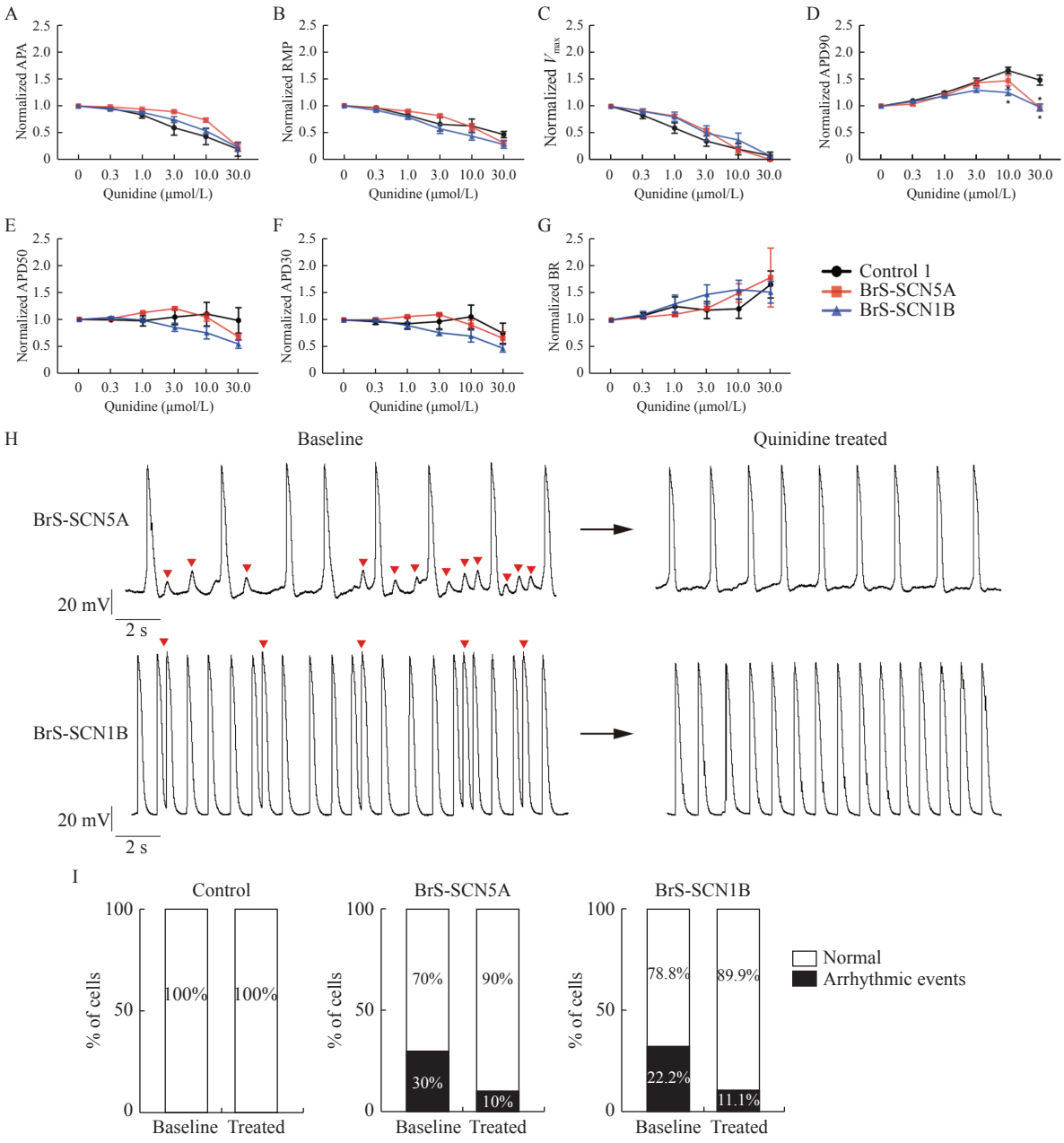

Fig. 5 **iPSC-CMs in response to escalating concentrations of quinidine.** A–G: Quinidine-treated CMs exhibited the reduction of APA (A), RMP (B), V_{max} (C), and the prolongation of APD90 (D) after standardization, while changes in APD50 (E) and APD30 (F) were modest. All the groups had comparable beating rate (BR) (G). Control: n=10; BrS-SCN5A: n=10; BrS-SCN1B: n=9. Values given are mean±SEM. $^*P$<0.05 *vs.* control (by paired t-test). H: Representative spontaneous AP traces. Left panels: BrS iPSC-CMs AP baseline with EADs and DADs (indicated by red arrows). Right panels: quinidine within 3-fold the ETPC can abolish baseline EADs. I: Percentage of cardiomyocytes displaying arrhythmic events at baseline and after treating with 10 μmol/L quinidine (Control: n=10; BrS-SCN5A: n=10; BrS-SCN1B: n=9, Chi-square test). iPSC-CMs: induced pluripotent stem cell-derived cardiomyocytes; APA: action potential amplitude; RMP: resting membrane potential; V_{max}: maximum upstroke velocity; APD: action potential duration; AP: Action potential; EADs: early after depolarizations; DADs: delayed after depolarizations.

CMs are more fetal-like in phenotype than adult cardiomyocytes, which has impeded the widespread use of iPSC-CMs for scientific studies[22–23]. Currently, prolonged culturing is the most accessible and easy approach for prompting cardiac maturation[24]. In the present study, the cells were cultivated for 60 days *in vitro*, till differentiation into a mature state. Our morphological analysis indicated that the structures of BrS-CMs were normal. On the other hand, the organized sarcomeres together with ultra-micro aligned Z-disc structures indicated that the D60 cardiomyocytes exhibited a high degree of maturity. We have reported that ion channel function relies on the iPSC-CM maturation status[25]. Thus, applying

such relatively mature CMs for disease modeling would be highly reliable.

Electrophysiological abnormalities caused by $Na_v1.5$ gene variations

Among BrS patients, *SCN5A* mutations are found in a quarter of patients[26]. Meanwhile, other gene mutations including *SCN1B* have been rarely reported[27–28]. Herein, iPSC-CMs carrying the *SCN1B* missense mutation (c.590C>T) also had a significant decrease in sodium current, although the decline was not as obvious as that of *SCN5A* mutant BrS-CMs. This could be explained by the fact that *SCN1B* encodes only the accessory subunit of the sodium channel[29].

Compared to I_{Na}, action potential can better reflect the impact of variants on the entire cellular electrophysiology, including the compensation of other ion channels to the sodium current impairment. Our study illuminated the abnormality in AP profiles of BrS-CMs, which is in line with previous studies[30]. The BrS-CMs also presented a prolonged AP duration. These characteristics are similar to those of iPS-CMs carrying SCN5A p.1795insD, which causes overlap between the syndromes of BrS and long QT phenotypes[27]. Moreover, BrS-CMs exhibited multiple abnormal calcium-related activities, including EAD-like and DAD-like events, which are thought to be a surrogate for polymorphic VT[31–32]. Collectively, both $Na_v1.5$ gene mutants in our study showed impaired electrophysiological function, triggering adverse events related to BrS clinical manifestations.

Pharmacologic responses to quinidine

The pharmacologic basis of treating BrS is aimed at rebalancing outward and inward currents of the epicardium, either by reducing the outward I_{to} current or increasing the inward I_{Ca} current[33]. Quinidine, a class IA antiarrhythmic agent with significant I_{to} blocking properties, is reported to reduce electrical heterogeneity, realize synchrony, and terminate phase 2 reentrant activity[34]. However, the efficacy of quinidine is controversial as it may induce prolongation of the QT interval, leading to ventricular arrhythmia[35–36]. Since BrS is a genetic condition, the discrepancy in drug responses may result from the different genetic backgrounds. In our study, we evaluated the effects of quinidine on BrS-CMs with different sodium channel gene variations. We found that all the cell lines showed depressed phase 0 depolarization after quinidine treatment. APD90 presented with a concentration-dependent prolongation caused by quinidine, which is the result of inhibition of sodium channel in phase 0 and potassium channel in phase 1 and 3. It is worth mentioning that the prolongation was more profound in the control cells. The downward trend appeared when the concentration reached 10 μmol/L, suggesting that the L-type calcium channel was blocked by quinidine at such a concentration[37]. There was no prominent effect on APD30 or APD50. These findings are in line with the drug experiment on human ventricular trabeculae[38] or drug tests using optical mapping[39], indicating the pronounced blockade of potassium current especially hERG. Besides, we observed that adverse events were reduced or at least not added in the range of 3-fold the ETPC of quinidine in BrS-CMs. These findings support the idea that quinidine is an effective and safe drug for BrS patients with genetic risk.

Limitation

First, genotype might not equal pathogenesis. A low prevalence of mutation carriers leads to an ambiguous relationship between genotype and phenotype. Patients in the absence of any mutation may have an anatomic structural variant in the right ventricular outflow tract that is sufficient for pathogenesis[40]. However, we believe that the genetic basis is an important contributor to the pathogenesis of BrS. It is reported that the expression heterogeneity in $Na_v1.5$ expression could determine the conduction heterogeneities in different regions[41]. Second, our present model can enable study on the cellular level, but not on the organ or tissue level. Previous studies performed in a canine ventricular wedge model successfully captured the BrS ECG pattern[42]. However, it is unable for iPSC-CMs from monolayer culture to achieve such potential difference *in vitro*. Hopefully, the pathophysiological changes recapitulated here can be coupled with new techniques for engineering heart tissue.

Conclusion

In summary, our study verified the pathogenicity of two novel mutations in diverse subunits of sodium channel (*SCN5A* c.4213G>A and *SCN1B* c.590C>T) using patient-specific iPSC-CMs. Both iPSC-CMs recapitulated similar phenotypes of impaired sodium channel on the cellular level, including deleterious I_{Na}, abnormal action potential parameters, increased arrhythmia events, and cardiotoxicity-free quinidine usage within safe dose. Our findings help to understand the mechanisms of BrS at the cellular level

and support patient-specific iPSC-CMs as a promising platform for therapeutic target exploration.

Acknowledgments

The work was supported by the Natural Science Foundation of Jiangsu Province of China (Grant No. BK20160134 to LW and BK20191071 to CC), National Natural and Science Foundation of China (Grant No. 81900295 to CC), and Special Foundation for Clinical Science and Technology of Jiangsu Province (Grant No. BE2017754 to HWC).

References

[1] Brugada P, Brugada J. Right bundle branch block, persistent ST segment elevation and sudden cardiac death: a distinct clinical and electrocardiographic syndrome: a multicenter report[J]. *J Am Coll Cardiol,* 1992, 20(6): 1391–1396.

[2] Antzelevitch C. Brugada syndrome[J]. *Pacing Clin Electrophysiol,* 2006, 29(10): 1130–1159.

[3] Brugada J, Brugada R, Brugada P. Pharmacological and device approach to therapy of inherited cardiac diseases associated with cardiac arrhythmias and sudden death[J]. *J Electrocardiol,* 2000, 33 Suppl 1: 41–47.

[4] Nordkamp LRAO, Postema PG, Knops RE, et al. Implantable cardioverter-defibrillator harm in young patients with inherited arrhythmia syndromes: a systematic review and meta-analysis of inappropriate shocks and complications[J]. *Heart Rhythm,* 2016, 13(2): 443–454.

[5] Sieira J, Brugada P. Management of Brugada syndrome 2016: should all high risk patients receive an ICD? All high-risk patients should receive an implantable cardiac defibrillator[J]. *Circ Arrhythm Electrophysiol,* 2016, 9(11): e004195.

[6] Gourraud JB, Barc J, Thollet A, et al. The Brugada syndrome: a rare arrhythmia disorder with complex inheritance[J]. *Front Cardiovasc Med,* 2016, 3: 9.

[7] Schulze-Bahr E, Eckardt L, Breithardt G, et al. Sodium channel gene (SCN5A) mutations in 44 index patients with Brugada syndrome: different incidences in familial and sporadic disease[J]. *Hum Mutat,* 2003, 21(6): 651–652.

[8] Risgaard B, Jabbari R, Refsgaard L, et al. High prevalence of genetic variants previously associated with Brugada syndrome in new exome data[J]. *Clin Genet,* 2013, 84(5): 489–495.

[9] Wang L, Han Z, Dai J, et al. Brugada syndrome caused by sodium channel dysfunction associated with a SCN1B variant A197V[J]. *Arch Med Res,* 2020, 51(3): 245–253.

[10] Yan GX, Antzelevitch C. Cellular basis for the Brugada syndrome and other mechanisms of arrhythmogenesis associated with ST-segment elevation[J]. *Circulation,* 1999, 100(15): 1660–1666.

[11] Wang Y, Liang P, Lan F, et al. Genome editing of isogenic human induced pluripotent stem cells recapitulates long QT phenotype for drug testing[J]. *J Am Coll Cardiol,* 2014, 64(5): 451–459.

[12] Jans D, Callewaert G, Krylychkina O, et al. Action potential-based MEA platform for *in vitro* screening of drug-induced cardiotoxicity using human iPSCs and rat neonatal myocytes[J]. *J Pharmacol Toxicol Methods,* 2017, 87: 48–52.

[13] Matsa E, Rajamohan D, Dick E, et al. Drug evaluation in cardiomyocytes derived from human induced pluripotent stem cells carrying a long QT syndrome type 2 mutation[J]. *Eur Heart J,* 2011, 32(8): 952–962.

[14] Selga E, Sendfeld F, Martinez-Moreno R, et al. Sodium channel current loss of function in induced pluripotent stem cell-derived cardiomyocytes from a Brugada syndrome patient[J]. *J Mol Cell Cardiol,* 2018, 114: 10–19.

[15] Liang P, Sallam K, Wu HD, et al. Patient-specific and genome-edited induced pluripotent stem cell-derived cardiomyocytes elucidate single-cell phenotype of Brugada syndrome[J]. *J Am Coll Cardiol,* 2016, 68(19): 2086–2096.

[16] Antzelevitch C, Brugada P, Borggrefe M, et al. Brugada syndrome: report of the second consensus conference[J]. *Heart Rhythm,* 2005, 2(4): 429–440.

[17] Priori SG, Wilde AA, Horie M, et al. HRS/EHRA/APHRS expert consensus statement on the diagnosis and management of patients with inherited primary arrhythmia syndromes: Document endorsed by HRS, EHRA, and APHRS in May 2013 and by ACCF, AHA, PACES, and AEPC in June 2013[J]. *Heart Rhythm,* 2013, 10(12): 1932–1963.

[18] Belhassen B, Viskin S, Fish R, et al. Effects of electrophysiologic-guided therapy with class IA antiarrhythmic drugs on the long-term outcome of patients with idiopathic ventricular fibrillation with or without the Brugada syndrome[J]. *J Cardiovasc Electrophysiol,* 1999, 10(10): 1301–1312.

[19] Probst V, Gourraud JB. Quinidine in Brugada syndrome: still a long way to go…[J]. *Circ Arrhythm Electrophysiol,* 2015, 8(6): 1309–1310.

[20] Malhi N, Cheung CC, Deif B, et al. Challenge and impact of quinidine access in sudden death syndromes: a national experience[J]. *JACC: Clin Electrophysiol,* 2019, 5(3): 376–382.

[21] Blinova K, Dang Q, Millard D, et al. International multisite study of human-induced pluripotent stem cell-derived cardiomyocytes for drug proarrhythmic potential assessment[J]. *Cell Rep,* 2018, 24(13): 3582–3592.

[22] Lieu DK, Fu JD, Chiamvimonvat N, et al. Mechanism-based facilitated maturation of human pluripotent stem cell-derived cardiomyocytes[J]. *Circ Arrhythm Electrophysiol,* 2013, 6(1): 191–201.

[23] Poon E, Yan B, Zhang S, et al. Transcriptome-guided functional analyses reveal novel biological properties and regulatory hierarchy of human embryonic stem cell-derived ventricular cardiomyocytes crucial for maturation[J]. *PLoS One,* 2013, 8(10): e77784.

[24] Kuppusamy KT, Jones DC, Sperber H, et al. Let-7 family of

microRNA is required for maturation and adult-like metabolism in stem cell-derived cardiomyocytes[J]. *Proc Natl Acad Sci U S A,* 2015, 112(21): E2785–E2794.

[25] Wang J, Cui C, Nan H, et al. Graphene sheet-induced global maturation of cardiomyocytes derived from human induced pluripotent stem cells[J]. *ACS Appl Mater Interfaces,* 2017, 9(31): 25929–25940.

[26] Kapplinger JD, Tester DJ, Alders M, et al. An international compendium of mutations in the SCN5A-encoded cardiac sodium channel in patients referred for Brugada syndrome genetic testing[J]. *Heart Rhythm,* 2010, 7(1): 33–46.

[27] Portero V, Casini S, Hoekstra M, et al. Anti-arrhythmic potential of the late sodium current inhibitor GS-458967 in murine *Scn5a*-1798insD$^{+/-}$ and human *SCN5A*-1795insD$^{+/-}$ iPSC-derived cardiomyocytes[J]. *Cardiovasc Res,* 2017, 113(7): 829–838.

[28] El-Battrawy I, Müller J, Zhao Z, et al. Studying Brugada syndrome with an SCN1B variants in human-induced pluripotent stem Cell-derived cardiomyocytes[J]. *Front Cell Dev Biol,* 2019, 7: 261.

[29] Malhotra JD, Chen C, Rivolta I, et al. Characterization of sodium channel α- and β-subunits in rat and mouse cardiac myocytes[J]. *Circulation,* 2001, 103(9): 1303–1310.

[30] Kosmidis G, Veerman CC, Casini S, et al. Readthrough-promoting drugs gentamicin and PTC124 fail to rescue nav1.5 function of human-induced pluripotent stem cell-derived cardiomyocytes carrying nonsense mutations in the sodium channel gene SCN5A[J]. *Circ Arrhythm Electrophysiol,* 2016, 9(11): e004227.

[31] Broyles CN, Robinson P, Daniels MJ. Fluorescent, bioluminescent, and optogenetic approaches to study excitable physiology in the single cardiomyocyte[J]. *Cells,* 2018, 7(6): 51.

[32] Kopljar I, Lu HR, Van Ammel K, et al. Development of a human iPSC cardiomyocyte-based scoring system for cardiac hazard identification in early drug safety de-risking[J]. *Stem Cell Rep,* 2018, 11(6): 1365–1377.

[33] Sieira J, Dendramis G, Brugada P. Pathogenesis and management of Brugada syndrome[J]. *Nat Rev Cardiol,* 2016, 13(12): 744–756.

[34] Belhassen B, Glick A, Viskin S. Efficacy of quinidine in high-risk patients with Brugada syndrome[J]. *Circulation,* 2004, 110(13): 1731–1737.

[35] Vicente J, Johannesen L, Mason JW, et al. Comprehensive T wave morphology assessment in a randomized clinical study of dofetilide, quinidine, ranolazine, and verapamil[J]. *J Am Heart Assoc,* 2015, 4(4): e001615.

[36] Hai JJ, Wong CK, Chan PH, et al. Quinidine for Brugada syndrome: panacea or poison?[J]. *HeartRhythm Case Rep,* 2016, 2(6): 486–490.

[37] Nishida A, Takizawa T, Matsumoto A, et al. Inhibition of ATP-sensitive K^+ channels and L-Type Ca^{2+} channels by amiodarone elicits contradictory effect on insulin secretion in MIN6 cells[J]. *J Pharmacol Sci,* 2011, 116(1): 73–80.

[38] Page G, Ratchada P, Miron Y, et al. Human ex-vivo action potential model for pro-arrhythmia risk assessment[J]. *J Pharmacol Toxicol Methods,* 2016, 81: 183–195.

[39] Pfeiffer-Kaushik ER, Smith GL, Cai B, et al. Electrophysiological characterization of drug response in hSC-derived cardiomyocytes using voltage-sensitive optical platforms[J]. *J Pharmacol Toxicol Methods,* 2019, 99: 106612.

[40] Szél T, Antzelevitch C. Abnormal repolarization as the basis for late potentials and fractionated electrograms recorded from epicardium in experimental models of Brugada syndrome[J]. *J Am Coll Cardiol,* 2014, 63(19): 2037–2045.

[41] Martin CA, Guzadhur L, Grace AA, et al. Mapping of reentrant spontaneous polymorphic ventricular tachycardia in a *Scn5a*$^{+/-}$ mouse model[J]. *Am J Physiol Heart Circ Physiol,* 2011, 300(5): H1853–H1862.

[42] Nishida K, Fujiki A, Mizumaki K, et al. Canine model of Brugada syndrome using regional epicardial cooling of the right ventricular outflow tract[J]. *J Cardiovasc Electrophysiol,* 2004, 15(8): 936–941.